

RESEARCH ARTICLE | SEPTEMBER 18 2024

# Sliding-reversible bandgap modulation in irreversible asymmetric multilayers

Changming Ke  ; Yudi Yang  ; Zhuang Qian; Shi Liu  

 Check for updates

*Appl. Phys. Lett.* 125, 122902 (2024)

<https://doi.org/10.1063/5.0232473>



Nanotechnology & Materials Science

Optics & Photonics

Impedance Analysis

Scanning Probe Microscopy

Sensors

Failure Analysis & Semiconductors



**Unlock the Full Spectrum.**  
From DC to 8.5 GHz.  
Your Application. Measured.

[Find out more](#)



# Sliding-reversible bandgap modulation in irreversible asymmetric multilayers

Cite as: Appl. Phys. Lett. **125**, 122902 (2024); doi: [10.1063/5.0232473](https://doi.org/10.1063/5.0232473)

Submitted: 7 August 2024 · Accepted: 10 September 2024 ·

Published Online: 18 September 2024



View Online



Export Citation



CrossMark

Changming Ke,<sup>1,2</sup>  Yudi Yang,<sup>1,2</sup>  Zhuang Qian,<sup>1,2</sup> and Shi Liu<sup>1,2,a)</sup> 

## AFFILIATIONS

<sup>1</sup>Department of Physics, School of Science and Research Center for Industries of the Future, Westlake University, Hangzhou, Zhejiang 310030, China

<sup>2</sup>Institute of Natural Sciences, Westlake Institute for Advanced Study, Hangzhou, Zhejiang 310024, China

<sup>a)</sup> Author to whom correspondence should be addressed: [liushi@westlake.edu.cn](mailto:liushi@westlake.edu.cn)

## ABSTRACT

The electronic bandgap of a material is often fixed after fabrication. The capability to realize on-demand and nonvolatile control over the bandgap will unlock exciting opportunities for adaptive devices with enhanced functionalities and efficiency. We introduce a general design principle for on-demand and nonvolatile control of bandgap values, which utilizes reversible sliding-induced polarization driven by an external electric field to modulate the irreversible background polarization in asymmetric two-dimensional (2D) multilayers. The structural asymmetry can be conveniently achieved in homobilayers of Janus monolayers and heterobilayers of nonpolar monolayers, making the design principle applicable to a broad range of 2D materials. We demonstrate the versatility of this design principle using experimentally synthesized Janus metal dichalcogenide multilayers as examples. Our first-principles calculations show that the bandgap modulation can reach up to 0.3 eV and even support a semimetal-to-semiconductor transition. By integrating a ferroelectric monolayer represented by  $1T''$ -MoS<sub>2</sub> into a bilayer, we show that the combination of intrinsic ferroelectricity and sliding ferroelectricity leads to multi-bandgap systems coupled to multi-step polarization switching. The sliding-reversible bandgap modulation offers an avenue to dynamically adjust the optical, thermal, and electronic properties of 2D materials through mechanical and electrical stimuli.

Published under an exclusive license by AIP Publishing. <https://doi.org/10.1063/5.0232473>

The bandgap, a fundamental property of materials, is crucial in determining their optical, thermal, and electrical behaviors.<sup>1</sup> It plays a key role in modern device physics and technology, determining the performance of a wide range of devices, like transistors, solar cells, and light-emitting diodes.<sup>2–5</sup> The ability to dynamically and nonvolatily adjust the bandgap is highly desirable, enabling real-time control of material properties. This opens up opportunities for “smart devices” that respond instantaneously to changes in environmental conditions or user inputs, thereby enhancing both functionality and efficiency.<sup>6</sup> For example, solar panels with tunable bandgaps could optimize their absorption characteristics to maximize efficiency throughout the day and in various weather conditions. Materials with temperature-sensitive bandgaps that regulate light and heat transmission in response to changing environmental conditions form the basis of smart windows.<sup>6</sup> Similarly, tunable laser diodes that allow on-demand control of their output wavelength may provide enhanced precision in procedures like laser surgery or scanning.<sup>7</sup> While techniques like doping,<sup>5,8</sup> strain,<sup>9</sup> and interface engineering<sup>10</sup> can effectively modify material bandgaps, these methods are typically static, meaning the bandgap

is fixed after fabrication. This poses a challenge for achieving dynamic and real-time control over bandgaps. Efforts for reversible bandgap tuning have mainly focused on phase-change materials<sup>11,12</sup> and electric field effect.<sup>13,14</sup> However, materials that exhibit robust, dynamic, and nonvolatile bandgap tunability are still relatively rare.

Two-dimensional (2D) van der Waals (vdW) materials can be stacked and relatively shifted. The interlayer motions like sliding and twisting offer a unique degree of freedom to tune the properties of these material, even inducing emergent phenomena not present in their individual layers.<sup>15–19</sup> For example, controlling the twist angle between layers can lead to the formation of long-wavelength moiré potential, effectively quenching the kinetic energy of electrons and enhancing the electronic correlation. This sets the stage for various exotic quantum phases, such as superconductivity<sup>20–22</sup> and Mott insulators.<sup>23–25</sup> In recent years, sliding ferroelectricity, a phenomenon where lateral sliding between nonpolar monolayers produces a switchable vertical polarization, has attracted great attention. Notable bilayer systems exhibiting sliding ferroelectricity that have been confirmed experimentally include bilayer boron nitride and transition metal

dichalcogenides.<sup>15,26–29</sup> This discovery expands the range of 2D ferroelectrics with out-of-plane polarization, potentially allowing for full utilization of atomic thickness in the development of ultrathin nanoelectronics. Various measures can induce interlayer sliding in layered vdW materials, including external electric field<sup>15,26,30</sup> and shear strain.<sup>31</sup>

Given the facile capability to induce interlayer sliding, sliding-induced bandgap modulation, if achievable, could significantly improve the methods available for real-time tuning of electronic structures. However, unlike twisting, sliding in bilayers of identical monolayers generally has a less significant impact on their electronic properties, as it does not substantially modulate the periodic potential landscape. Here, we present a general strategy that integrates a reversible polarization arising from sliding ( $\mathcal{P}_s$ ) with a background out-of-plane polarization ( $\mathcal{P}_{bg}$ ) that does not need to be reversible (switchable), to achieve sliding-tunable bandgaps in a vdW multilayer.

Taking a bilayer as an example (Fig. 1), the background polarization may result from the structural asymmetry of the monolayer, such as in a homobilayer of Janus materials. It could also arise from charge transfer between nonpolar monolayers with different work functions in a heterobilayer. In both cases, the direction of  $\mathcal{P}_{bg}$  is *not* reversible by an electric field. Another key requirement for the bilayer configuration is that it should support sliding ferroelectricity, which can be conveniently achieved based on the general theory for bilayer stacking ferroelectricity.<sup>32</sup> For a bilayer with both  $\mathcal{P}_{bg}$  and  $\mathcal{P}_s$ , the sliding allows transition between two states with different out-of-plane polarization, a high-polarization (HP) state with  $\mathcal{P}_{bg} - \mathcal{P}_s$  and a low-polarization (LP) state with  $\mathcal{P}_{bg} + \mathcal{P}_s$ . Since the depolarization field within the bilayer is directly coupled to the magnitude of the out-of-plane polarization and can strongly affect the bandgap,<sup>33–35</sup> the two polar states can possess substantially different bandgaps, enabling sliding-induced, nonvolatile tuning of the electronic structures.

We demonstrate this design principle using density functional theory (DFT) calculations, focusing on the well-known family of 2D materials, transition metal dichalcogenides (TMDs),<sup>36,37</sup> many of which have already been synthesized experimentally. We find that a Janus hexagonal (1H)  $AXY$  ( $A = \text{Mo}, \text{W}$ ;  $X, Y = \text{S}, \text{Se}, \text{Te}$ ) bilayer with parallel stacking, denoted as the  $p + p$  configuration [Fig. 1(a)], can exhibit a reversible bandgap change of 0.1–0.2 eV. Moreover, a sliding-driven semimetal–semiconductor transition is realized in the tetragonal (1T) WTeSe bilayer. Additionally, the magnitude of

bandgap modulation can be further enhanced by increasing the layer number. Specifically, the sliding-induced bandgap change in the trilayer 1H-WTeSe reaches up to 0.3 eV. The design principle is also applicable to a heterobilayer consisting of nonpolar monolayers, denoted as  $np + np'$  [Fig. 1(b)], as exemplified by 1H-WSe<sub>2</sub>/1H-MoX<sub>2</sub> ( $X = \text{S}, \text{Se}, \text{Te}$ ). Finally, we show that in a bilayer consisting of recently synthesized ferroelectric 1T<sup>''</sup>-MoS<sub>2</sub> and nonpolar 1H-MoS<sub>2</sub> ( $f + np$  configuration), it is possible to achieve a multi-bandgap system coupled to multi-step polarization switching. The design principle proposed in this work for on-demand control of bandgaps is versatile and opens up opportunities for voltage-configurable multi-state electronics.

DFT calculations are performed using the Vienna *ab initio* Simulation Package VASP.<sup>38,39</sup> The exchange–correlation interaction is described by the Perdew–Burke–Ernzerhof (PBE) functional<sup>40</sup> and Heyd–Scuseria–Ernzerhof hybrid density functional (HSE06),<sup>41</sup> with Grimme’s D3 dispersion correction.<sup>42</sup> The projector augmented wave (PAW) method<sup>43</sup> is used to describe the electron–ion interaction between the core ion and valence electrons. The plane wave kinetic energy cutoff is 600 eV, and a  $9 \times 9 \times 1$  Monkhorst–Pack grid is used to sample the Brillouin zone for the unit cell. A vacuum region of thickness more than 20 Å is included to avoid interactions between periodic images. The climbing image nudged elastic band (CL-NEB) method<sup>44</sup> is employed to identify minimum energy pathways, with electronic energy and atomic force converged to  $10^{-7}$  eV and 0.01 eV/Å, respectively. The dipole correction method, as proposed by Neugebauer and Scheffler,<sup>45</sup> is considered in all calculations. Detailed parameters are available at <https://github.com/kechangming/Sliding-Bandgap>.

We start with a heuristic approach to understand the bandgap modulation caused by the interlayer sliding in a homobilayer consisting of two polar Janus monolayers. As depicted in Fig. 2(a), the surface polarization bound charges associated with the out-of-plane polarization generate a depolarization field that opposes the polarization. This field establishes a potential step that scales with the magnitude of polarization, thereby differentiating the electronic states of the two polar surfaces. Electrons near the  $\mathcal{P}^-$  surface naturally have higher energy due to increased Coulomb repulsion, which defines the valence band maximum (VBM). Conversely, the conduction band minimum (CBM) is located at the  $\mathcal{P}^+$  surface. The depolarization field resembles the built-in electric field within the depletion region of a  $p$ - $n$  junction.

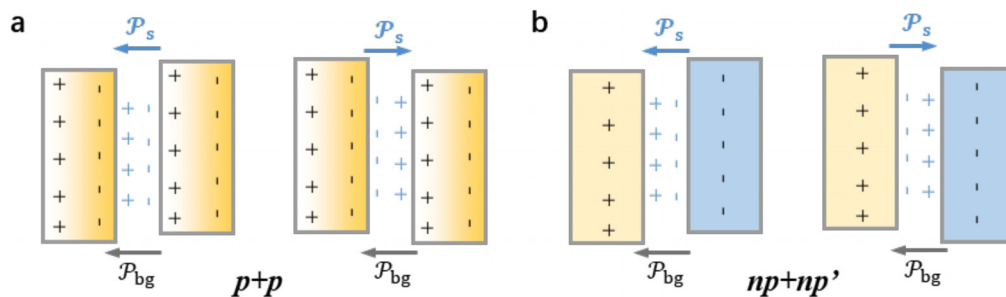


**FIG. 1.** Design principle for sliding-reversible bandgap modulation in asymmetric bilayers. Here,  $p$  denotes a polar layer such as a Janus monolayer,  $np$  a nonpolar layer, and  $np'$  a different nonpolar layer. (a)  $p + p$  stacking with the background polarization  $\mathcal{P}_{bg}$  arising from the intrinsic asymmetry of the monolayer. (b)  $np + np'$  stacking with  $\mathcal{P}_{bg}$  resulting from charge transfer due to the work function difference. The yellow layer is the low-work function layer, and the blue layer is the high-work function layer. In both cases,  $\mathcal{P}_{bg}$  is not reversible, while  $\mathcal{P}_s$  is reversible by interlayer sliding.

Although the polarization direction of Janus monolayers,  $\mathcal{P}_{bg}$ , are not reversible, the polarization arising from the stacking,  $\mathcal{P}_s$ , can be flipped by sliding. Therefore, the effective potential step across the bilayer in the HP state with  $\mathcal{P}_{bg} + \mathcal{P}_s$  is higher than that in the LP state with  $\mathcal{P}_{bg} - \mathcal{P}_s$ . This results in a larger bandgap in the LP state.

The simple band bending model discussed above is corroborated by our DFT calculations of 2D Janus TMDs, many of which, like MoSeS and WSeS, have already been synthesized.<sup>46,47</sup> As a case study, we focus on the 1H-MoSSe bilayer. In the AB-stacking configuration, as illustrated in Fig. 2(c), electrons transfer from the upper Mo layer to the lower Se layer due to the greater electronegativity of Se relative to Mo. This leads to an upward  $\mathcal{P}_s$  that runs along  $\mathcal{P}_{bg}$  and thus a HP state. Band structure calculations with PBE reveal a bandgap of  $E_g^{HP} = 1.48$  eV. Sliding the bottom layer by 1/3 of a unit cell reverses the charge transfer direction [see Fig. 2(d)], resulting in a LP state and a higher bandgap of  $E_g^{LP} = 1.58$  eV. Therefore, a bandgap modulation  $\Delta E_g = 0.1$  eV is achieved in the 1H-MoSSe bilayer. We further perform calculations for 1H-WSSe, WTeSe, MoSSe, and MoTeSe bilayers, with the bandgap values computed with PBE and HSE06 reported in Fig. 2(e). It is evident that the bandgap modulation driven by sliding is a robust phenomenon common to all studied bilayers. It is important to note that the energies of the HP and LP states may differ, with  $E_{HP} - E_{LP}$  ranging from 3 to 6 meV per unit cell, as shown in Fig. 2(e). However, despite this difference, these structures remain switchable by an electric field, as observed in the MoS<sub>2</sub>/WS<sub>2</sub> heterobilayer ferroelectrics,<sup>28</sup> where the value of  $E_{HP} - E_{LP}$  is 2 meV per unit cell. Besides the 1H phase with trigonal prismatic coordination, 2D TMDs may also crystallize in the 1T phase featuring tetragonal symmetry and octahedral coordination of the transition metal. Interestingly, we find that the bilayer 1T-WTeSe undergoes a

semiconductor-to-semimetal transition during the sliding from a LP state to a HP state, as depicted in Fig. 2(f).

The magnitude of  $\Delta E_g$  can be enhanced in multilayers by promoting the contribution of reversible  $\mathcal{P}_s$  to the total polarization. For a trilayer 1H-MoSSe, it may adopt “ladder ferroelectricity” where each pair of neighboring monolayers supports stacking ferroelectricity.<sup>48</sup> As illustrated in Fig. 3(a), an ABC stacked trilayer has two interfaces possessing parallel upward  $\mathcal{P}_s$ . Applying a sliding gradient, where the middle layer slides one-third of a unit cell and the bottom layer slides two-thirds of a unit cell, will change the stacking from ABC to CBA, switching the direction of  $\mathcal{P}_s$  at both interfaces and resulting in a LP state [see the change in charge density in Fig. 3(b)]. Our DFT calculations confirm that the ABC configuration, characterized by an out-of-plane polarization of 18.6 pC/m, has a PBE bandgap of 0.13 eV. In contrast, the polarization in the CBA-stacked trilayer decreases to 16.7 pC/m, and the bandgap widens to 0.33 eV. The magnitude of  $\Delta E_g$  in this trilayer is 0.2 eV, doubling the 0.1 eV observed in the bilayer. Additionally, atom-resolved band structures [Fig. 3(c)] confirm that the VBM and CBM are dominated by states of the bottom  $\mathcal{P}^-$  layer and the top  $\mathcal{P}^+$  layer, respectively, consistent with the schematic illustrated in Figs. 2(a) and 2(b). As summarized in Fig. 3(d) for several Janus trilayers, the value of  $\Delta E_g$  ranges from 0.2 to 0.3 eV, improving upon those in bilayers. Specifically, HSE06 predicts a bandgap modulation of  $\approx 0.3$  eV and a direct-to-indirect bandgap transition in the trilayer 1H-WTeSe.

The proposed design principle does not rely on polar monolayers for two reasons. First, the built-in field resulting from the work function difference between the constituent monolayers in a heterobilayer can serve as the origin of  $\mathcal{P}_{bg}$ .<sup>49</sup> Second, a distinct feature of sliding ferroelectrics is that the stacking of nonpolar monolayers can also

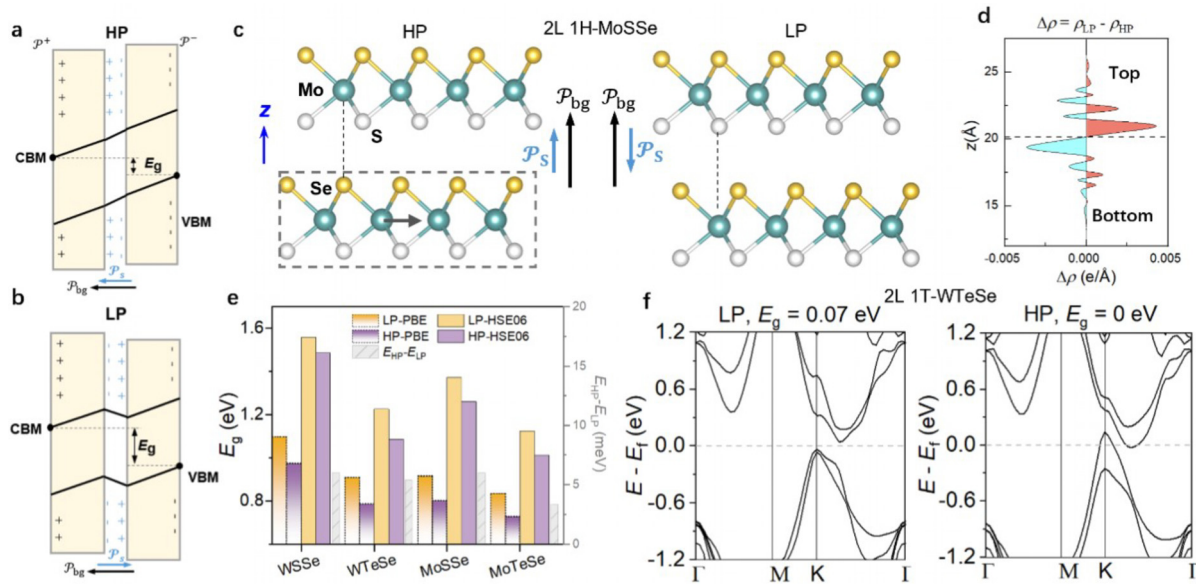


**FIG. 2.** Sliding-reversible bandgap modulation in Janus TMD homobilayers of  $p + p$  configuration. Schematics of band alignments in (a) high-polarization (HP) and (b) low-polarization (LP) states. (c) Configurations of bilayer (2L) 1H-MoSSe showing sliding-induced flip of  $\mathcal{P}_s$  from  $+z$  to  $-z$ . (d) Sliding-induced interlayer charge transfer along the  $z$  direction, with  $\Delta\rho$  representing the difference in electronic charge density between LP and HP states ( $\Delta\rho > 0$  indicates an increase in electron density). (e) Bandgap values and energy differences between HP and LP states ( $E_{HP} - E_{LP}$ ) for bilayer 1H-WSSe, WTeSe, MoSSe, and MoTeSe, computed with PBE and HSE06. (f) Sliding-induced semiconductor–semimetal transition in 2L 1T-WTeSe, with band structures computed using HSE06.

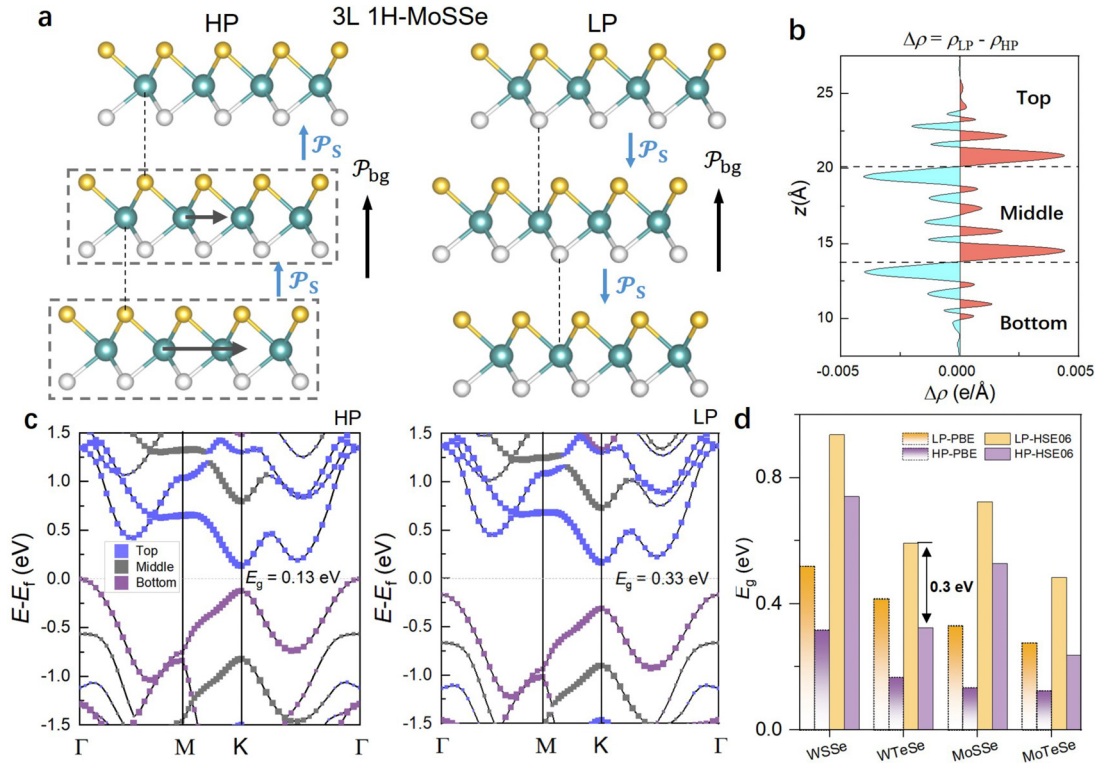


**FIG. 3.** Enhanced reversible bandgap modulation in Janus trilayers. (a) Configurations of trilayer (3L) 1H-MoSSe illustrating the transition from ABC-stacking to CBA-stacking by a sliding gradient. The directions of  $\mathcal{P}_s$  at both interfaces are flipped. (b) Sliding-induced interlayer charge transfer in the  $z$  direction. A positive  $\Delta\rho$  value means an increase in electron density. (c) Atom-resolved band structures in 3L 1H-MoSSe. (d) Bandgap values for trilayer 1H-WSSe, WTeSe, MoSSe, and MoTeSe at different polarization states.

generate vertical polarization as long as the stacking satisfies the symmetry requirement.<sup>32</sup> The mechanism of bandgap modulation in an  $np + np'$  heterobilayer is sketched in Figs. 4(a) and 4(b), which differs subtly from the  $p + p$  stacking. The charge transfer between monolayers pushes down the valence states in the low-work function layer and raises the conduction states in the high-work function layer. Since the VBM and CBM are located in the low-work function and high-work function layers, respectively, stronger charge transfer causes the VBM and CBM to move further apart. In the LP state, the sliding-induced  $\mathcal{P}_s$  tends to suppress charge transfer between monolayers, leading to a smaller bandgap. Conversely, in the HP state where  $\mathcal{P}_s$  promotes charge transfer, the bandgap is larger. It is important to note that the correlation between  $E_g$  and the magnitude of total polarization is exactly **opposite** to that in homobilayers of the  $p + p$  configuration.

Our DFT investigations of 1H-WSe<sub>2</sub>/1H-AX<sub>2</sub> ( $A = \text{Mo}, \text{W}; X = \text{S}, \text{Se}, \text{Te}$ ) bilayers confirm the model analysis discussed above, revealing that the HP state indeed has a larger bandgap, with the values of  $\Delta E_g$  ranging from 0.09 to 0.14 eV, as shown in Fig. 4(d). The projected density of states (PDOS) diagrams in Figs. 4(e) and 4(f) for 1H-WSe<sub>2</sub>/1H-WS<sub>2</sub> heterobilayer show a clear upward shift of the CBM of the high-work function layer in HP states, consistent with schematics in Figs. 4(a) and 4(b).

A potential issue for a heterobilayer is the lattice mismatch-induced formation of moiré patterns, which could complicate the control over sliding ferroelectricity. We suggest that doping presents a

viable solution to mitigate the mismatch and enhance control. For instance, the lattice mismatch between 1H-WTe<sub>2</sub> (with an in-plane lattice constant  $a_{\text{IP}}^{\text{WTe}_2} = 3.52 \text{ \AA}$ ) and 1H-WSe<sub>2</sub> ( $a_{\text{IP}}^{\text{WSe}_2} = 3.30 \text{ \AA}$ ) can be significantly reduced by doping 1H-WSe<sub>2</sub> with Te atoms ( $a_{\text{IP}}^{\text{WSeTe}} = 3.40 \text{ \AA}$ ). This doping approach is feasible, as our design principle does not require an ordered arrangement of Te dopants within the lattice. We perform a set of model calculations for 1H-AX<sub>2</sub>/1H-AXTe ( $A = \text{Mo}, \text{W}; X = \text{S}, \text{Se}$ ), where 1H-AXTe approximates a (homogeneously) Te-doped nonpolar monolayer [Fig. 4(g), not a polar Janus monolayer]. Similar to the undoped heterobilayer, the HP state consistently exhibits a larger bandgap than the LP state [Fig. 4(h)], further confirming the robustness of the design principle.

Reversible and precisely tunable multi-state switching is essential for enabling high-density information storage and neuromorphic computing applications.<sup>50,51</sup> Finally, we demonstrate that combining a 2D ferroelectric with a nonpolar monolayer (denoted as  $f + np$ ) presents a compelling route to achieve fine-tuned and nonvolatile control over multiple bandgaps using voltage. In this bilayer, there are three types of polarization:  $\mathcal{P}_f$  originating from monolayer's ferroelectricity,  $\mathcal{P}_{\text{bg}}$  due to the work function difference, and  $\mathcal{P}_s$  arising from sliding ferroelectricity. This leads to four polar states in this bilayer system:  $\mathcal{P}_{\text{bg}} - \mathcal{P}_f - \mathcal{P}_s$ ,  $\mathcal{P}_{\text{bg}} - \mathcal{P}_f + \mathcal{P}_s$ ,  $\mathcal{P}_{\text{bg}} + \mathcal{P}_f - \mathcal{P}_s$ , and  $\mathcal{P}_{\text{bg}} + \mathcal{P}_f + \mathcal{P}_s$ , labeled as  $\mathcal{P}^{-,-}$ ,  $\mathcal{P}^{-,+}$ ,  $\mathcal{P}^{+,-}$ , and  $\mathcal{P}^{+,+}$ , respectively. We focus on a possible experimental realization of such a bilayer system, specifically a 1H-MoS<sub>2</sub>/1T'<sup>'''</sup>-MoS<sub>2</sub> heterojunction. It is noted

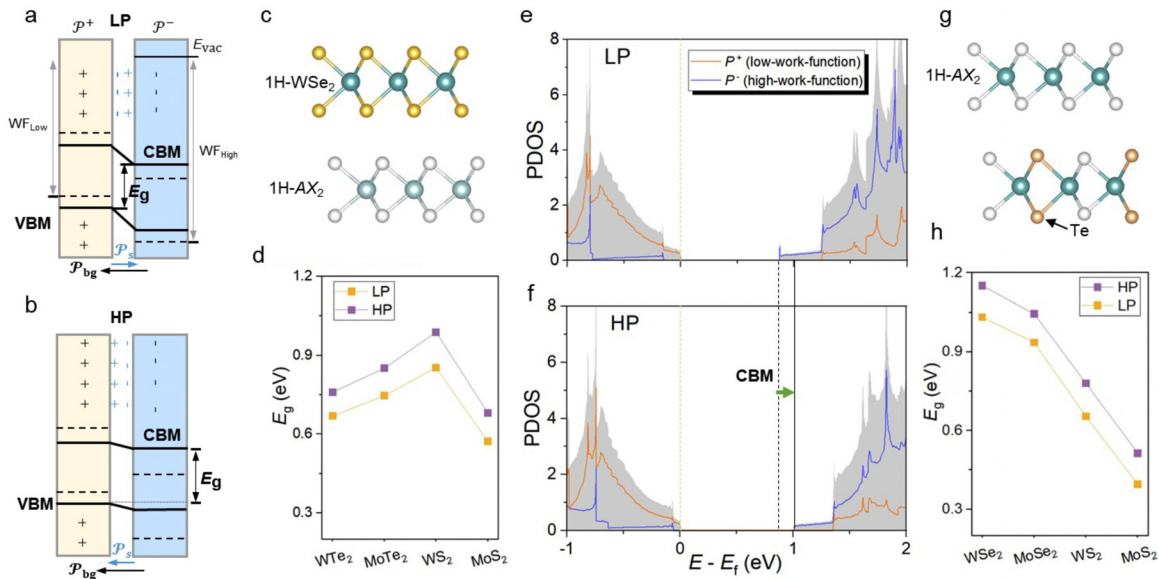


**FIG. 4.** Sliding-reversible bandgap modulation in heterobilayers consisting of two nonpolar monolayers ( $np + np'$ ). Schematics of band alignments in (a) low-polarization (LP) and (b) high-polarization (HP) states. The dashed lines represent the intrinsic CBM and VBM before charge transfer. The yellow and blue layers have low-work function ( $WF_{Low}$ ) and high-work function ( $WF_{High}$ ), respectively. (c) Atomic structure of  $1H-WSe_2/1H-AX_2$  ( $A = Mo, W, X = S, Te$ ). (d) Bandgap values for  $1H-WSe_2/1H-AX_2$  bilayers in HP and LP states computed with PBE. Projected density of states (PDOS) of (e) LP and (f) HP states for  $1H-WSe_2/1H-WSe_2$  heterobilayer. (g) Atomic structure of an asymmetrically doped (quasi-)homobilayer consisting of  $1H-AX_2$  ( $A = W, Mo; X = S, Se$ ) and its homogeneously Te-doped nonpolar monolayer  $1H-AXTe$ . The bandgap values are reported in (h).

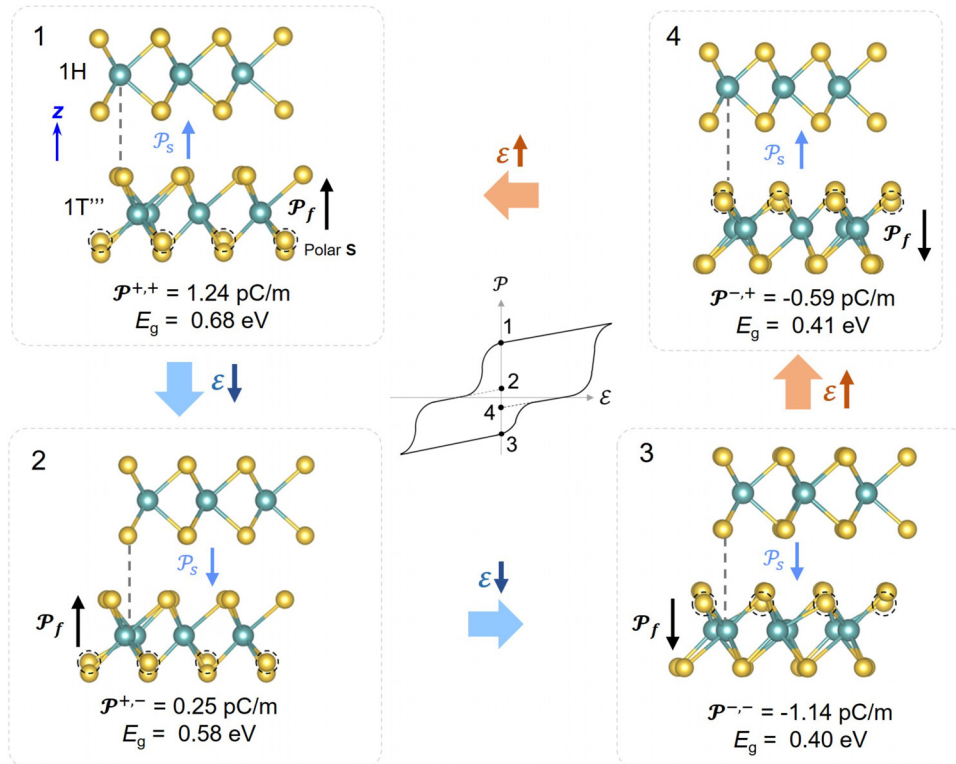


**FIG. 5.** On-demand voltage control of multiple bandgap values in a  $1H-MoS_2/1T''-MoS_2$  heterojunction, supporting both monolayer ferroelectricity ( $\mathcal{P}_f$ ) and sliding ferroelectricity ( $\mathcal{P}_s$ ). Monolayer ferroelectricity arises from intralayer charge transfer involving polar sulfur (S) atoms, which are highlighted with dotted circles.

that  $1T''$ -MoS<sub>2</sub> featuring a switchable out-of-plane polarization has been experimentally synthesized recently.<sup>52</sup> The minimum energy pathways for the reversal processes of  $\mathcal{P}_f$  and  $\mathcal{P}_s$  are identified using the DFT-based NEB technique, respectively. The barrier for switching  $\mathcal{P}_f$  is 0.043 eV/atom, higher than the 0.012 eV/atom required for switching  $\mathcal{P}_s$ . This difference likely translates to multi-step polarization switching under an applied electric field ( $\mathcal{E}$ ). Starting at the  $\mathcal{P}^{++}$  state, the bandgap evolves from 0.68 to 0.58 eV at the partially switched  $\mathcal{P}^{+-}$  state, and then becomes 0.40 eV at the fully reversed  $\mathcal{P}^{--}$  state (Fig. 5). Applying an opposite electric field can recover the  $\mathcal{P}^{++}$  state eventually. The multi-step polarization switching under an applied electric field, coupled to the corresponding changes in multiple bandgap values, highlights the potential for developing multi-state memory devices.

In summary, we have demonstrated a general design principle to realize reversible and nonvolatile bandgap modulation by taking advantage of both sliding ferroelectricity and structural asymmetry in 2D multilayers. The irreversible background polarization arising from the structural asymmetry is modulated by the reversible polarization due to sliding, leading to polar states with different polarization magnitudes and thereby varying built-in depolarization fields that strongly affect the electronic structures. A notable advantage of this design principle is that it is applicable to both homobilayers of polar monolayers as well as heterobilayers of nonpolar monolayers. Based on experimentally synthesized 2D Janus materials, we demonstrate substantial bandgap modulations up to 0.3 eV. The introduction of ferroelectric monolayer such as  $1T''$ -MoS<sub>2</sub> into a bilayer to enable switchable background polarization allows for on-demand control of multiple bandgap values via voltage, offering exciting opportunities for adaptive electronics and multi-state memory devices.

This work is supported by National Natural Science Foundation of China (Nos. 12304128 and 12074319) and Westlake Education Foundation. The computational resource was provided by Westlake HPC Center.

## AUTHOR DECLARATIONS

### Conflict of Interest

The authors have no conflicts to disclose.

### Author Contributions

Changming Ke and Yudi Yang contributed equally to this work.

**Changming Ke:** Conceptualization (equal); Data curation (equal); Funding acquisition (equal); Investigation (equal); Methodology (equal); Visualization (equal); Writing – original draft (equal); Writing – review & editing (equal). **Yudi Yang:** Data curation (equal); Investigation (equal). **Zhuang Qian:** Data curation (supporting); Investigation (supporting). **Shi Liu:** Methodology (equal); Software (equal); Supervision (equal); Writing – original draft (equal); Writing – review & editing (equal).

### DATA AVAILABILITY

The data that supports the findings of this study are available within the article.

## REFERENCES

- N. W. Ashcroft and N. D. Mermin, *Solid State Physics* (Brooks Cole, 1976).
- S. M. Sze and K. K. Ng, *Physics of Semiconductor Devices* (John Wiley & Sons, Ltd, 2006).
- A. Chaves, J. G. Azadani, H. Alsalman, D. R. da Costa, R. Frisenda, A. J. Chaves, S. H. Song, Y. D. Kim, D. He, J. Zhou, A. Castellanos-Gomez, F. M. Peeters, Z. Liu, C. L. Hinkle, S.-H. Oh, P. D. Ye, S. J. Koester, Y. H. Lee, P. Avouris, X. Wang, and T. Low, "Bandgap engineering of two-dimensional semiconductor materials," *npj 2D Mater. Appl.* **4**, 29 (2020).
- J. B. Varley, B. Shen, and M. Higashiwaki, "Wide bandgap semiconductor materials and devices," *J. Appl. Phys.* **131**, 230401 (2022).
- C.-Z. Ning, L. Dou, and P. Yang, "Bandgap engineering in semiconductor alloy nanomaterials with widely tunable compositions," *Nat. Rev. Mater.* **2**, 17070 (2017).
- Y. Zhou, F. Fan, Y. Liu, S. Zhao, Q. Xu, S. Wang, D. Luo, and Y. Long, "Unconventional smart windows: Materials, structures and designs," *Nano Energy* **90**, 106613 (2021).
- J. Buus, M.-C. Amann, and D. J. BlumenthalSze, *Tunable Laser Diodes and Related Optical Sources* (Wiley-IEEE Press, 2005).
- Y. Chen, J. Xi, D. O. Dumcenco, Z. Liu, K. Suenaga, D. Wang, Z. Shuai, Y.-S. Huang, and L. Xie, "Tunable band gap photoluminescence from atomically thin transition-metal dichalcogenide alloys," *ACS Nano* **7**, 4610 (2013).
- M. L. Lee, E. A. Fitzgerald, M. T. Bulsara, M. T. Currie, and A. Lochtefeld, "Strained Si, SiGe, and Ge channels for high-mobility metal-oxide-semiconductor field-effect transistors," *J. Appl. Phys.* **97**, 011101 (2005).
- H. Kroemer, "Nobel lecture: Quasielectric fields and band offsets: Teaching electrons new tricks," *Rev. Mod. Phys.* **73**, 783 (2001).
- W. Dong, H. Liu, J. K. Behera, L. Lu, R. J. H. Ng, K. V. Sreekanth, X. Zhou, J. K. W. Yang, and R. E. Simpson, "Wide bandgap phase change material tuned visible photonics," *Adv. Funct. Mater.* **29**, 1806181 (2019).
- P. Prabhathan, K. V. Sreekanth, J. Teng, J. H. Ko, Y. J. Yoo, H.-H. Jeong, Y. Lee, S. Zhang, T. Cao, C.-C. Popescu, B. Mills, T. Gu, Z. Fang, R. Chen, H. Tong, Y. Wang, Q. He, Y. Lu, Z. Liu, H. Yu, A. Mandal, Y. Cui, A. S. Ansari, V. Bhingardive, M. Kang, C. K. Lai, M. Merklein, Y. M. Song, Z. Tian, J. Hu, M. Losurdo, A. Majumdar, X. Miao, X. Chen, B. Gholipour, K. A. Richardson, B. J. Eggleton, M. Wuttig, and R. Singh, "Roadmap for phase change materials in photonics and beyond," *iScience* **26**, 107946 (2023).
- Y. Zhang, T.-T. Tang, C. Girit, Z. Hao, M. C. Martin, A. Zettl, M. F. Crommie, Y. R. Shen, and F. Wang, "Direct observation of a widely tunable bandgap in bilayer graphene," *Nature* **459**, 820 (2009).
- E. V. Castro, K. S. Novoselov, S. V. Morozov, N. M. R. Peres, F. Guinea, A. K. Geim, and A. H. C. Neto, "Biased bilayer graphene: Semiconductor with a gap tunable by the electric field effect," *Phys. Rev. Lett.* **99**, 216802 (2007).
- M. V. Stern, Y. Waschitz, W. Cao, I. Nevo, K. Watanabe, T. Taniguchi, E. Sela, M. Urbakh, O. Hod, and M. B. Shalom, "Interfacial ferroelectricity by van der Waals sliding," *Science* **372**, 1462 (2021).
- M. Wu and J. Li, "Sliding ferroelectricity in 2D van der Waals materials: Related physics and future opportunities," *Proc. Natl. Acad. Sci. U. S. A.* **118**, e2115703118 (2021).
- T. Cui, K. Yip, A. Hassan, G. Wang, X. Liu, Y. Sun, and T. Filletter, "Graphene fatigue through van der Waals interactions," *Sci. Adv.* **6**, eabb1335 (2020).
- S. Pakdel, A. Rasmussen, A. Taghizadeh, M. Kruse, T. Olsen, and K. S. Thygesen, "High-throughput computational stacking reveals emergent properties in natural van der Waals bilayers," *Nat. Commun.* **15**, 932 (2024).
- N. Ding, J. Chen, C. Gui, H. You, X. Yao, and S. Dong, "Phase competition and negative piezoelectricity in interlayer-sliding ferroelectric ZrI<sub>2</sub>," *Phys. Rev. Mater.* **5**, 084405 (2021).
- Y. Cao, V. Fatemi, S. Fang, K. Watanabe, T. Taniguchi, E. Kaxiras, and P. Jarillo-Herrero, "Unconventional superconductivity in magic-angle graphene superlattices," *Nature* **556**, 43 (2018).
- G. Chen, A. L. Sharpe, P. Gallagher, I. T. Rosen, E. J. Fox, L. Jiang, B. Lyu, H. Li, K. Watanabe, T. Taniguchi, J. Jung, Z. Shi, D. Goldhaber-Gordon, Y. Zhang, and F. Wang, "Signatures of tunable superconductivity in a trilayer graphene moiré superlattice," *Nature* **572**, 215 (2019).
- M. Yankowitz, S. Chen, H. Polshyn, Y. Zhang, K. Watanabe, T. Taniguchi, D. Graf, A. F. Young, and C. R. Dean, "Tuning superconductivity in twisted bilayer graphene," *Science* **363**, 1059 (2019).

- <sup>23</sup>G. Chen, L. Jiang, S. Wu, B. Lyu, H. Li, B. L. Chittari, K. Watanabe, T. Taniguchi, Z. Shi, J. Jung, Y. Zhang, and F. Wang, "Evidence of a gate-tunable mott insulator in a trilayer graphene moiré superlattice," *Nat. Phys.* **15**, 237 (2019).
- <sup>24</sup>Y. Shimazaki, I. Schwartz, K. Watanabe, T. Taniguchi, M. Kroner, and A. Imamoglu, "Strongly correlated electrons and hybrid excitons in a moiré heterostructure," *Nature* **580**, 472 (2020).
- <sup>25</sup>Y. Cao, V. Fatemi, A. Demir, S. Fang, S. L. Tomarken, J. Y. Luo, J. D. Sanchez-Yamagishi, K. Watanabe, T. Taniguchi, E. Kaxiras, R. C. Ashoori, and P. Jarillo-Herrero, "Correlated insulator behaviour at half-filling in magic-angle graphene superlattices," *Nature* **556**, 80 (2018).
- <sup>26</sup>K. Yasuda, X. Wang, K. Watanabe, T. Taniguchi, and P. Jarillo-Herrero, "Stacking-engineered ferroelectricity in bilayer boron nitride," *Science* **372**, 1458 (2021).
- <sup>27</sup>Z. Zheng, Q. Ma, Z. Bi, S. de la Barrera, M.-H. Liu, N. Mao, Y. Zhang, N. Kiper, K. Watanabe, T. Taniguchi, J. Kong, W. A. Tisdale, R. Ashoori, N. Gedik, L. Fu, S.-Y. Xu, and P. Jarillo-Herrero, "Unconventional ferroelectricity in moiré heterostructures," *Nature* **588**, 71 (2020).
- <sup>28</sup>L. Rogée, L. Wang, Y. Zhang, S. Cai, P. Wang, M. Chhowalla, W. Ji, and S. P. Lau, "Ferroelectricity in untwisted heterobilayers of transition metal dichalcogenides," *Science* **376**, 973 (2022).
- <sup>29</sup>D. Wu, M. G. Lagally, and F. Liu, "Stabilizing graphitic thin films of wurtzite materials by epitaxial strain," *Phys. Rev. Lett.* **107**, 236101 (2011).
- <sup>30</sup>E. Y. Tsymlal, "Two-dimensional ferroelectricity by design," *Science* **372**, 1389 (2021).
- <sup>31</sup>J. Liu, C. Zhu, Z. Zhang, Q. Ren, X. Zhang, Y. Zhang, Y. Jin, W. Qiu, H. Wang, J. Zhao, and P. Zhao, "Interlayer shear coupling in bilayer graphene," *npj 2D Mater. Appl.* **6**, 38 (2022).
- <sup>32</sup>J. Ji, G. Yu, C. Xu, and H. J. Xiang, "General theory for bilayer stacking ferroelectricity," *Phys. Rev. Lett.* **130**, 146801 (2023).
- <sup>33</sup>X. Duan, J. Huang, B. Xu, and S. Liu, "A two-dimensional multiferroic metal with voltage-tunable magnetization and metallicity," *Mater. Horiz.* **8**, 2316 (2021).
- <sup>34</sup>C. Ke, J. Huang, and S. Liu, "Two-dimensional ferroelectric metal for electrocatalysis," *Mater. Horiz.* **8**, 3387 (2021).
- <sup>35</sup>J. Huang, X. Duan, S. Jeon, Y. Kim, J. Zhou, J. Li, and S. Liu, "On-demand quantum spin hall insulators controlled by two-dimensional ferroelectricity," *Mater. Horiz.* **9**, 1440 (2022).
- <sup>36</sup>S. Manzeli, D. Ovchinnikov, D. Pasquier, O. V. Yazyev, and A. Kis, "2D transition metal dichalcogenides," *Nat. Rev. Mater.* **2**, 17033 (2017).
- <sup>37</sup>D. Voiry, A. Mohite, and M. Chhowalla, "Phase engineering of transition metal dichalcogenides," *Chem. Soc. Rev.* **44**, 2702 (2015).
- <sup>38</sup>G. Kresse and J. Furthmüller, "Efficient iterative schemes for ab initio total energy calculations using a plane-wave basis set," *Phys. Rev. B* **54**, 11169 (1996).
- <sup>39</sup>G. Kresse and J. Furthmüller, "Efficiency of ab-initio total energy calculations for metals and semiconductors using a plane-wave basis set," *Comput. Mater. Sci.* **6**, 15 (1996).
- <sup>40</sup>J. P. Perdew, K. Burke, and M. Ernzerhof, "Generalized gradient approximation made simple," *Phys. Rev. Lett.* **77**, 3865 (1996).
- <sup>41</sup>A. V. Krueger, O. A. Vydrov, A. F. Izmaylov, and G. E. Scuseria, "Influence of the exchange screening parameter on the performance of screened hybrid functionals," *J. Chem. Phys.* **125**, 224106 (2006).
- <sup>42</sup>S. Grimme, J. Antony, S. Ehrlich, and H. Krieg, "A consistent and accurate ab initio parametrization of density functional dispersion correction (DFT-D) for the 94 elements H-Pu," *J. Chem. Phys.* **132**, 154104 (2010).
- <sup>43</sup>P. E. Blochl, "Projector augmented-wave method," *Phys. Rev. B* **50**, 17953 (1994).
- <sup>44</sup>G. Henkelman, B. P. Uberuaga, and H. Jónsson, "A climbing image nudged elastic band method for finding saddle points and minimum energy paths," *J. Chem. Phys.* **113**, 9901 (2000).
- <sup>45</sup>J. Neugebauer and M. Scheffler, "Adsorbate-substrate and adsorbate-adsorbate interactions of Na and K adlayers on Al(111)," *Phys. Rev. B* **46**, 16067 (1992).
- <sup>46</sup>A.-Y. Lu, H. Zhu, J. Xiao, C.-P. Chuu, Y. Han, M.-H. Chiu, C.-C. Cheng, C.-W. Yang, K.-H. Wei, Y. Yang, Y. Wang, D. Sokaras, D. Nordlund, P. Yang, D. A. Muller, M.-Y. Chou, X. Zhang, and L.-J. Li, "Janus monolayers of transition metal dichalcogenides," *Nat. Nanotechnol.* **12**, 744 (2017).
- <sup>47</sup>M. S. G. Feuer, A. R.-P. Montblanch, M. Y. Sayyad, C. M. Purser, Y. Qin, E. M. Alexeev, A. R. Cadore, B. L. T. Rosa, J. Kerfoot, E. Mostaani, R. Kaleba, P. Kolari, J. Kopaczek, K. Watanabe, T. Taniguchi, A. C. Ferrari, D. M. Kara, S. Tongay, and M. Atatüre, "Identification of exciton complexes in charge-tunable Janus WSeS monolayers," *ACS Nano* **17**, 7326 (2023).
- <sup>48</sup>S. Deb, W. Cao, N. Raab, K. Watanabe, T. Taniguchi, M. Goldstein, L. Kronik, M. Urbakh, O. Hod, and M. Ben Shalom, "Cumulative polarization in conductive interfacial ferroelectrics," *Nature* **612**, 465 (2022).
- <sup>49</sup>Y. Luo, S. Wang, H. Shu, J.-P. Chou, K. Ren, J. Yu, and M. Sun, "A MoSSe/blue phosphorene vdW heterostructure with energy conversion efficiency of 19.9% for photocatalytic water splitting," *Semicond. Sci. Technol.* **35**, 125008 (2020).
- <sup>50</sup>T. Li, Y. Wu, G. Yu, S. Li, Y. Ren, Y. Liu, J. Liu, H. Feng, Y. Deng, M. Chen, Z. Zhang, and T. Min, "Realization of sextuple polarization states and interstate switching in antiferroelectric CuInP<sub>2</sub>S<sub>6</sub>," *Nat. Commun.* **15**, 2653 (2024).
- <sup>51</sup>S. Prosdandev and L. Bellaiche, "THz-induced activation of hidden states in rare-earth-doped BiFeO<sub>3</sub> solid solutions," *Phys. Rev. Mater.* **6**, 116201 (2022).
- <sup>52</sup>C. HuangFu, Y. Zhou, C. Ke, J. Liao, J. Wang, H. Liu, D. Liu, S. Liu, L. Xie, and L. Jiao, "Out-of-plane ferroelectricity in two-dimensional 1T<sup>′</sup>-MoS<sub>2</sub> above room temperature," *ACS Nano* **18**, 14708 (2024).